AIAA JOURNAL
Vol. 45, No. 9, September 2007

Blast-Wave Dynamics in a Circular Duct with a Sudden Expansion

Shen-Min Liang*
Far-East University of Technology, Hsin-Shih, Tainan County, Taiwan, Republic of China
and
Chi-Yao Liao†
Chung-Chou Institute of Technology, Yuan-Lin, Chang-Hua County, Taiwan, Republic of China

DOI: 10.2514/1.27151

In this study, the problem of a planar blast wave in a duct with a sudden expansion is considered. An incident blast wave that contains two shock waves is arranged so that one pair of vortex rings induced by the first shock wave interacts with the second shock wave of the blast wave and with the reflected shock associated with the first shock wave. A high-resolution Euler/Navier–Stokes solver using a fifth-order weighted essentially nonoscillation scheme is employed to investigate the problem. After the Euler/Navier–Stokes solver is validated to be reasonably accurate, the flow fields induced by the shock/vortex interactions are investigated by computational shadowgraph and computational schlieren techniques. It is found that the trajectories formed by major ring-vortex centers may be different case by case, depending on the arrival time sequence of the second shock wave and the reflected shock wave. In particular, a third vortex ring may be developed, causing the trajectory's turn at some critical time in viscous-flow models. Because of viscous dissipation, consequently stronger vortex-ring strength predicted by the inviscid-flow model than that for the viscous-flow model can result in 14–32% lower pressures at the major ring-vortex centers in the inviscid flow compared with the turbulent flow during the time interval investigated for case A, and 20–32% for case B, and 21–38% for case C. Because of the boundary layer development along the duct wall after the sudden expansion, the reflection type of the first shock wave is changed from a regular reflection in the inviscid-flow case to a single Mach reflection that directly affects the arrival time of the reflected shock wave at the sharp corner. Moreover, the mechanism of the vortex ring formation based on the inviscid-flow model is analyzed. It is found that the term due to the dilation effect also plays a more important role in vorticity generation than the baroclinic term.

Nomenclature

c	=	speed of sound
D	=	duct diameter
e	=	total energy per unit volume
F	=	flux vector in axial direction
G	=	flux vector in radial direction
H	=	source term for axis symmetry
M_S	=	incident shock/blast-wave Mach number
p	=	pressure
R	=	duct radius
Re	=	Reynolds number
r	=	radial direction
S_1	=	blast-wave front (first shock)
S_2	=	second shock
t	=	time
V	=	vortex ring
$\boldsymbol{V}$	=	velocity vector, $\boldsymbol{V} = (V_r, V_\theta, V_z)$
z	=	axial direction
Γ	=	circulation
ρ	=	density
$\boldsymbol{\omega}$	=	vorticity vector
∇	=	gradient operator, $\nabla = \hat{e}_r \frac{\partial}{\partial r} + \frac{1}{r}\hat{e}_\theta \frac{\partial}{\partial \theta} + \hat{e}_z \frac{\partial}{\partial z}$
∇^2	=	Laplacian operator, $\nabla^2 = \frac{\partial^2}{\partial r^2} + \frac{1}{r}\frac{\partial}{\partial r} + \frac{1}{r^2}\frac{\partial^2}{\partial \theta^2} + \frac{\partial^2}{\partial z^2}$

Received 14 August 2006; revision received 4 May 2007; accepted for publication 7 May 2007.

*Professor, Department of Computer Application Engineering. Associate Fellow AIAA.

†Associate Professor, Department of Mechanical and Computer-Aided Engineering.

I. Introduction

IN GENERAL, when energy is rapidly released in a local region, a blast wave is produced and propagates outward either in a planar, cylindrical or spherical form. A blast wave generally has a structure composed of a primary shock front, expansion waves, and a second shock wave. In one direction the blast wave eventually becomes an N wave. Generally speaking, when a planar shock wave diffracts around a sharp expansion corner, it results in a contact surface, an expanded shock wave, an induced vortex, and expansion waves issuing from the corner for a two-dimensional problem [1–3]. When a blast wave is discharged from a small circular duct into a large one, blast-wave diffraction will occur at the sudden expansion. Because of the primary shock wave inducing a spiral ring vortex, consequently, the second shock/ring-vortex interaction occurs downstream of the sudden expansion. Moreover, the confined space will make the flow downstream the sudden expansion more complicated than that for an unconfined space, because a reflected shock wave associated with the primary shock occurs in the large duct.

The basic problem of shock-wave reflection from a wedge has been extensively investigated in the past. Ben-Dor [4] catalogued the type of shock-wave reflection from a wedge for different gases in his book. The wave reflection type theoretically depends on the shock Mach number M_S and the wedge angle. Takayama and Jiang [5] summarized the numerical and experimental results of shock-wave reflection over wedges from many researchers. For the problem of shock-wave diffraction around a sharp expansion corner, Sun and Takayama [6,7] studied the formation of a second shock wave behind the shock wave diffracting around a two-dimensional convex corner for different incident shock Mach numbers ranging from 1.03 to 1.74 in air. The second-shock wave is formed due to the existence of a locally supersonic flow. They found that the critical shock Mach number for the formation of the second-shock is 1.346. Kim and Setoguchi [8] experimentally studied a weak shock discharged from the open end of a duct with shock Mach number ranging 1.02 to 1.45. Jiang et al. [9] numerically and experimentally investigated the

evolution of a transmitting shock-wave and its associated primary vortex loop. Abate and Shyy [10] reviewed experimental and numerical results to highlight the flow phenomena and main physical mechanism associated with confined shocks undergoing a sudden expansion. Many others papers [11–14] are omitted to mention because of space limitation.

For shock/vortex interactions, many papers have also been published in literature [15–19]. Only some papers are referenced here. Meadows et al. [20] and Ellzey et al. [21] performed numerical studies on the interaction of a planar shock wave and vortex with various strengths. Gruichard et al. [22] modeled a shock wave interacting with a single vortex and with a pair of vortices by solving the Navier–Stokes equations, and resolved the deformation of the incident shock wave. Moreover, they also noted that the vortex was intensified and compressed in the direction normal to the shock and bent according to the curvature of the shock. Chaterjee [23] studied the phenomenon of an initially planar shock wave interacting with a compressible vortex by using a high-resolution shock-capturing scheme, and proposed a simple physical model based on the principle of shock-wave reflection to explain a complex shock structure formation and its dependence on the relative strengths of the interacting vortex and shock wave. Inoue and Takahashi [24] numerically studied the development of a flow field and the generation of sound due to the interaction between a vortex ring and a shock wave. Chang and Kim [25] presented numerical results for shock tube simulations coupled with a sudden area expansion. Jiang et al. [26] described experimental and numerical simulations of a circular shock tube generating a flow that underwent a sudden expansion, and presented complex transient shock-wave phenomena such as shock-wave reflection, shock/vortex interaction, and shock-wave focusing.

Blast waves/vortex interactions are closely related with shock/vortex interactions. Chen and Liang [27] found the fourth sound generated by a planar blast/vortex interaction, but not in the case of shock/vortex interaction. For a blast/vortex interaction, the second shock/vortex interaction plays an important role in the vorticity generation process. Kleine et al. [28] reviewed the processes and flow features that were observed when a shock wave diffracted at a sharp 90 deg corner. A detailed comparison of numerical and experimental results has made it possible to identify and clarify some small-scale structure within the flow. Their result gives the interpretation of the appearance of the second shock system and the evolution of the flow pattern with increasing shock Mach number. Sun and Takayama [7] reported on vorticity production in shock-wave diffraction over sharp convex corners for incident shock Mach numbers ranging from 1.05 to 1.7 at an increment of 0.1, and convex corner angles from 15 to 180 deg at an increment of 15 deg. They found that large corner angles always enhance the vorticity production for all shock strengths investigated. The vorticity production increases sharply for corner angles changing from 15 to 45 deg.

The aforementioned phenomena, such as vorticity production, shock/vortex interactions, and second-shock development, and so on, are important aspects of fluid mixing. The present work will make a further detailed study of blast/vortex interactions in a circular duct with three particular values of the expansion ratio by numerical simulation. To analyze the complicated flow structure, we will use the computational schlieren, computational shadowgraph, and computational holographic interferogram methods for flow field visualization.

The problem studied is briefly described here. A small circular duct is connected with a larger duct of radius (R), resulting in a sudden expansion defined to be $z = 0$. The small duct is $0.6R$ long, and the larger duct is $2R$ long. The centerline of the duct is defined at $r = 0$. The larger duct's diameter ($D = 2R$) is chosen to be a characteristic length. Initially ($t = 0$), a narrow region of width $0.005R$, bounded by two diaphragms and filled with high-pressure (p_1) air, is located upstream at a distance of $0.5R$ from the sudden expansion. This duct configuration is referred as case A. Outside the high-pressure region, the flow is quiescent and the pressure is at one standard atmosphere (p_0) which is chosen as a reference condition for variable normalization. The temperatures in the low- and high-pressure regions are initially the same. As $t > 0$, two diaphragms break and produce two blast waves which propagate upstream and downstream. The downstream moving blast wave is of interest, and will propagate through the sudden expansion, resulting in a reflected shock wave from the larger duct wall. Different values of the initial pressure ratio will be chosen to produce different strengths of downstream moving blast waves. By changing duct's expansion ratio, we will investigate the vortex ring, induced by the primary shock front, interacting with the second shock and the reflected shock in the larger duct in different time sequences, respectively.

II. Mathematical Formation and Numerical Method

A. Governing Equations

Neglecting the effects of external forces and heat transfer, the governing equations for axisymmetric duct flow are the equations of the mass, continuity, and energy. They can be expressed in a dimensionless, conservative form as

$$\frac{\partial Q}{\partial t} + \frac{\partial G}{\partial r} + \frac{\partial F}{\partial z} + H = \frac{\partial G_v}{\partial r} + \frac{\partial F_v}{\partial z} + H_v \tag{1}$$

where $Q = [\rho, \rho V_r, \rho V_z, e]^t$ is the conservative–variable vector, F, G the flux vector components, H the term due to the symmetry, and H_v the term associated with the flow viscous properties. Note that the dimensionless time variable is defined as $t = \tilde{t}c_0/D$, where $\tilde{t}$ is the dimensional time variable, and c_0 the speed of sound in the lower pressure region at $t = 0$. The detail of Eq. (1) can be found in [29]. For taking turbulence into account, the Baldwin–Lomax turbulence model [30] is used. To explore the mechanism of vorticity generation, the vorticity transport equation is used:

$$\frac{D\boldsymbol{\omega}}{Dt} = (\boldsymbol{\omega} \cdot \nabla)\boldsymbol{V} - \boldsymbol{\omega}(\nabla \cdot \boldsymbol{V}) - \frac{\nabla p \times \nabla \rho}{\rho^2} + \text{other terms} \tag{2}$$

Here $\boldsymbol{\omega}$ is the curl of the velocity $\boldsymbol{V} = [V_r, V_\theta, V_z]^t$, and other terms denote some terms associated the viscosity, which reduce to a single term $Re^{-1}\nabla^2\boldsymbol{\omega}$ for incompressible flow, where Re represents the Reynolds number. For a two-dimensional, inviscid flow, Eq. (2) reduces to

$$\frac{D\boldsymbol{\omega}}{Dt} = -\boldsymbol{\omega}(\nabla \cdot V) - \frac{\nabla p \times \nabla \rho}{\rho^2} \tag{3}$$

because the vorticity vector is perpendicular to the velocity vector. The first term on the right-hand side denotes the dilation effect, and the second term the baroclinic effect.

B. Numerical Method

A 5th-order weighted essentially nonoscillatory (WENO) scheme of Jiang and Shu [31] is used for spatial discretization, and a non-TVD 4th-order Runge–Kutta scheme of Shu and Osher [32] for time integration. On the wall, the slip condition is imposed for inviscid flows, and the nonslip condition for viscous flows. Because the problem of interest is axisymmetric, a half domain is considered for saving computational time. Thus a symmetric boundary condition is imposed on the duct centerline. On the upstream and downstream boundaries, a nonreflecting boundary condition of Thompson [33] is prescribed. The Courant number is chosen to be 0.6 for fast computation.

III. Results and Discussions

A. Code Validation

Six test flow problems [34] were tested. 1) A shock tube problem with the pressure ratio of 10 and the density ratio of 8 was considered. Our computed pressure and density distributions coincided excellently with the exact solution. 2) Laminar shock/boundary layer interaction at an inflow Mach number of 2, incident angle of 32.6 deg, and Reynolds number of 296,000 was investigated. The computed wall pressure and skin friction distributions reasonably

Table 1 Values of flow parameters chosen for numerical simulation

Mach number at sudden expansion, M_S	p_1/p_0	Arrival time of the 1st shock, t_1[a]		Arrival time of the 2nd shock, t_2[a]		Arrival time of the reflected shock, t_3[a]	
		Case A	Case C	Case A	Case C	Case A	Case C
1.05	5	1.9	——	2.5	——	5.6	——
1.2	16	1.7	1.6	2.7	2.5	5.4	2.4
1.3	30	1.6	1.4	2.9	2.7	5.3	2.3
1.4	49	1.4	1.3	3.1	3.0	5.2	2.2
1.5	72	1.2	1.2	3.4	3.4	5.2	2.1

[a]Note that t_1 denotes the dimensionless time required for the first shock arriving at the sudden expansion; similarly, for t_2 and t_3.

agreed with the experimental data of Hakkinen et al. [35]. 3) A planar shock wave diffracting around a 90 deg sharp convex corner for the incident shock Mach number $M_S = 1.5$ was studied. Our computational holograph was in good agreement with the experimental result of Yang [36]. 4) A subsonic flow over a flat plate at a Mach number of 0.5 and $Re = 2 \times 10^6$ was computed. The computed turbulent boundary layer profiles at several stations were in good agreement with the result in [37]. 5) The problem of a planar shock-wave propagation in a circular duct with a sudden expansion at $M_S = 1.5$ and an expansion ratio of 3 was investigated. Through a qualitative comparison, our computational schlieren picture, using the commercial Tecplot software package [38], was in good agreement with the result of Jiang [26]. 6) Finally, a problem of blast-wave reflection from a wedge at an initial pressure ratio of 4.641, a wedge angle of 27 deg, and $Re = 5 \times 10^6$ was explored. It was found that the computed density distribution along the flat plate agreed satisfactorily with the experimental result of Deschambault and Glass [39].

B. Case A: Problem of a Circular Duct with a Sudden Expansion

The geometry of the flow problem has been mentioned in the introduction. The intensity of the blast wave produced depends on the initial pressure ratio p_1/p_0. Let M_S represent the Mach number of the primary shock front of the blast wave at the sudden expansion. Let t_1, t_2, t_3 be the dimensionless arrival times of the primary, second, and reflected shock waves at the sudden expansion ($z = 0$), respectively. Table 1 shows the arrival times of these three shock waves corresponding to different blast-wave intensities. In case A, the duct's expansion ratio is 2, producing the second shock wave arriving at the sudden expansion earlier than the reflected shock wave. We will subsequently investigate case B in which the second and reflected shocks simultaneously arrive at the induced ring, and case C for the reflected shock wave arriving at the sudden expansion earlier than the second shock wave. The duct's expansion ratio is 1.57 for case B and 1.23 for case C. The M_S value ranges from 1.05 to 1.5 and 5 to 72 for the corresponding initial pressure ratio. Only two cases of $M_S = 1.3$ and $M_S = 1.5$ are reported here. To understand a basic overall flow structure, the inviscid-flow model is employed. A study of the grid-independence Euler solution for the case of $p_1/p_0 = 72$ on grids with grid sizes of 0.05, 0.01, and 0.001 has been made. It was found the intermediate-grid solution is almost the same as the fine-grid solution. Thus the intermediate grid is used for other cases.

Figure 1 shows computational schlieren pictures of the Euler solution at different instants for $M_S = 1.3$, a weak blast wave, and $M_S = 1.5$, a stronger blast wave. For the case of $M_S = 1.3$, from Fig. 1a one can see that at $t = 2.6$, the primary shock wave diffracts around the sudden expansion and the second shock arrives near the sudden expansion. At $t = 3.0$, the second shock is diffracting around the sudden expansion. At $t = 3.4$, the primary shock wave starts to be reflected from the larger duct wall. At $t = 3.8$, the reflected shock

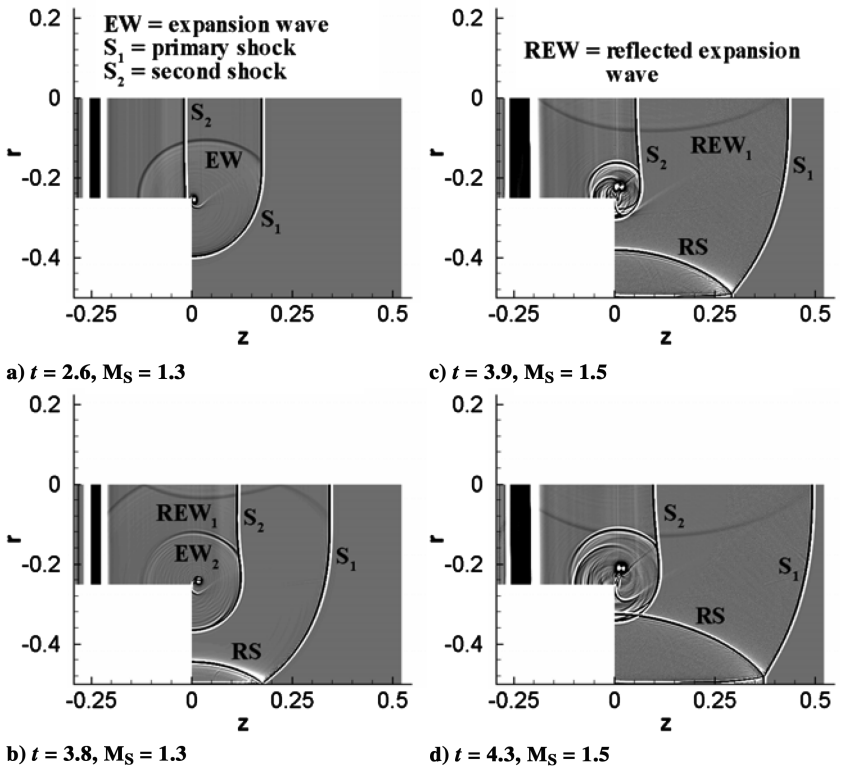

Fig. 1 Computational shadowgraphs at different instants for an inviscid-flow model (case A).

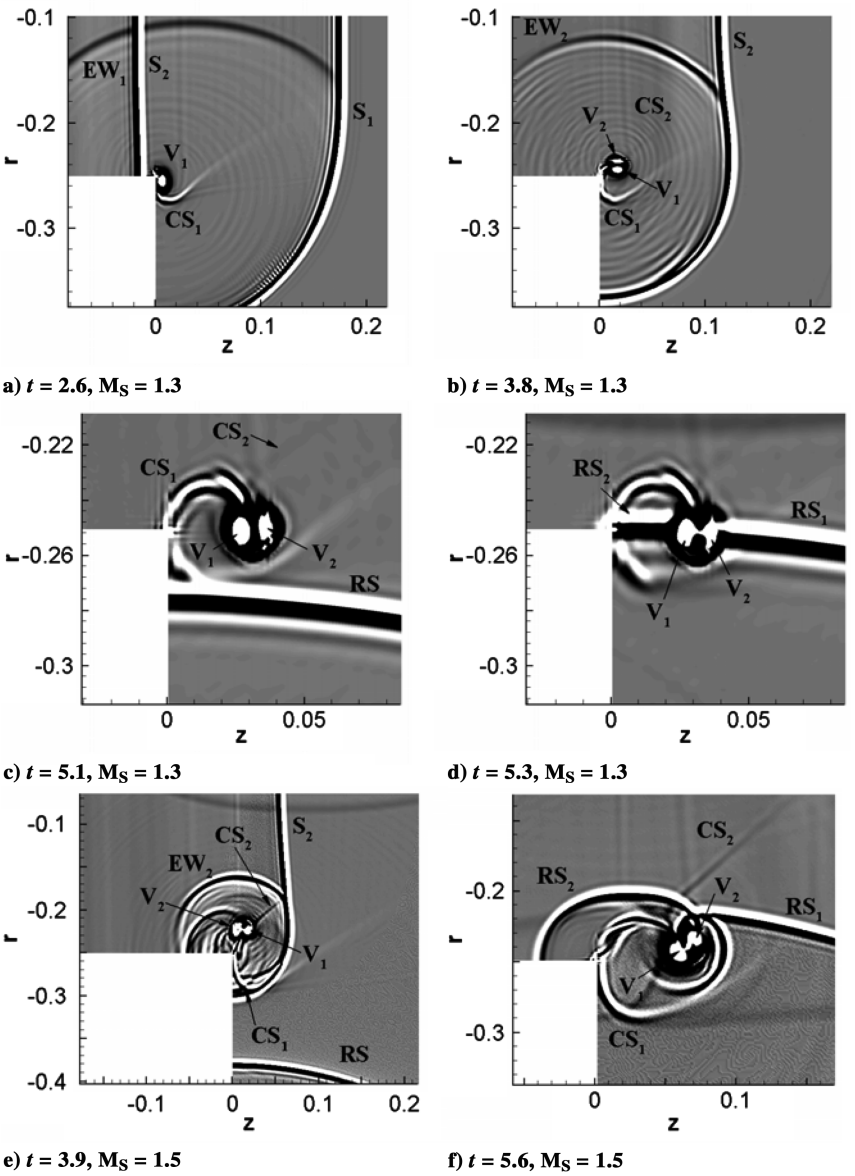

Fig. 2 Computational shadowgraphs of local flow fields near the sudden expansion at different instants (case A).

(RS) associated with the primary shock wave can be clearly seen, as shown in Fig. 1b. For the case of $M_S = 1.5$, similar phenomena as Figs. 1a and 1b occur. For a stronger blast wave, a contact surface is more visible than that in a weak blast wave. Moreover, the type of shock-wave reflection can be changed from a regular reflection to a single Mach reflection, as shown in Figs. 1c and 1d. Generally speaking, blast-wave diffraction around a 90 deg sharp corner, a pair of ring vortices can be induced in an axisymmetric case, as clearly seen from Figs. 1c and 1d. These two vortex rings, consisting of a major one and a minor one, have a different rotational direction. The major ring vortex rotates in a counterclockwise direction from a planar viewpoint, and a clockwise direction for the minor ring vortex. To see the flow fields induced by the second and reflected shock waves interacting with the induced vortices, a close look at the local flows is helpful.

Figure 2 shows the local flow structures near the sudden expansion for $M_S = 1.3$ and 1.5. First we discuss the $M_S = 1.3$ case. From Fig. 2a, we see the contact surface (CS_1) associated with the primary shock wave, both the induced major vortex ring, and circular expansion waves (EW_1). Later the second shock wave has passed the pair of induced vortex rings indicated by V_1 and V_2. Because of wave diffraction, expansion waves (EW_2) associated with the second shock wave are generated. As time advances, the second shock wave moves downstream and expansion waves (EW_2) grow circularly, as shown in 2b. At $t = 5.1$, the reflected shock wave (RS_1) moves closely to the pair of vortex rings, as shown in Fig. 2c. At $t = 5.2$, the reflected shock (RS_1) is starting to interact with the pair of vortex rings. At $t = 5.3$, the reflected shock (RS_1) is interacting with the pair of vortex rings, as shown in Fig. 2d. At $t = 5.4$, the reflected shock (RS_1) has just passed the pair of vortex rings. Next, we discuss the $M_S = 1.5$ case. Similar flow phenomena as in the $M_S = 1.3$ case occur. However, more complicated flow structures induced by the second shock wave result. It was found that the circular expansion waves can be clearly seen in the $M_S = 1.3$ case, but not in the $M_S = 1.5$ case. Moreover, the reflected shock wave (RS_1) in the $M_S = 1.5$ case is significantly distorted after interaction with the pair of induced vortex rings compared with that in the $M_S = 1.3$ case, as shown in Figs. 2e and 2f.

We have seen the global and local flow structures for blast waves passing the sudden expansion in Figs. 1 and 2. Because the induced two ring vortices need not have the same intensity, here we only report on the effect of the second shock wave passing through the major vortex ring. A quantitative result of the influence of the second shock wave with different intensities after interaction on the induced vortex rings is depicted in Fig. 3. This shows the variation of the minimum pressures at the major vortex centers with time for a fixed value of the initial pressure ratio. For the case of $p_1/p_0 = 6$, the blast wave produced is weak. The weak shock/ring-vortex interaction

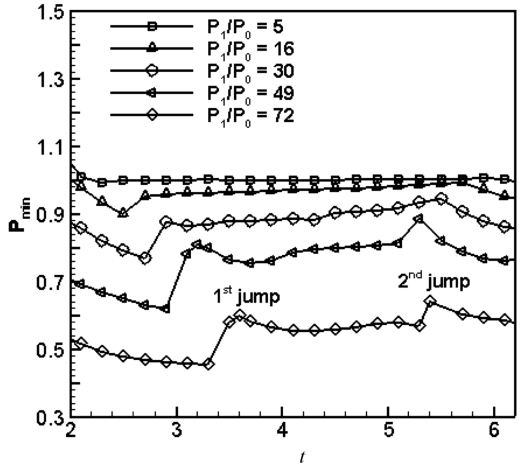

Fig. 3 Histories of the pressures at the major ring vortex centers from $t = 2.1$ to 6.1 with $\Delta t = 0.2$ for different blast-wave intensities (case A).

results in no significant effect on the primary ring-vortex strength. Thus the minimum pressures at the major vortex centers, not the vortex-ring center, are almost constant when the second shock wave has passed the two vortex rings. As blast-wave intensity increases, a first jump in the minimum pressure due to the passage of the second shock wave through the two vortex rings occurs. It is found that before the second shock interacts with the two vortex rings, the minimum pressures at the primary vortex centers are as low as 0.570 for $M_S = 1.3$ ($p_1/p_0 = 30$), and 0.828 for $M_S = 1.5$ ($p_1/p_0 = 72$). After interaction, the minimum pressure is increased to 0.641 for $M_S = 1.3$, and 0.887 for $M_S = 1.5$, because the major vortex ring is weakened by the reflected shock. For other blast-wave intensities, the pressure variation at the major vortex center is shown in Fig. 3. The stronger the blast wave, the bigger the first jump. Moreover, a second jump can occur when the reflected shock wave (RS_1) passes through the pair of vortex rings for stronger blast waves with $p_1/p_0 \geq 49$. Namely, the passage of a shock wave through a vortex can weaken the vortex strength. The second shock wave has larger influence on the ring-vortex strength than the reflected shock. We thought the reflected shock wave is weaker than the second shock wave.

From Fig. 3, we also see that the major vortex center pressures are decreased with the blast-wave intensity. In other words, the stronger the blast wave, the lower the vortex-center pressures induced.

The locations of the ring's vortex centers are also affected by the second and reflected shock waves, which start from the corner of the sudden expansion. Figure 4 shows the vortex center's location for different blast-wave intensities. At earlier times, the major vortex centers move downstream and toward the larger duct wall, because of the effect of the expanded diffracted shock wave. At some critical time, the primary vortex centers move toward the duct centerline. This is due to the growth of the minor vortex ring, after the passage of the second shock wave through the pair of vortex rings induced by the first shock wave. For example, the minor vortex ring (V_2) grows almost as the major vortex ring (V_1) in size, as shown in Fig. 4 for the cases of $M_S = 1.3$ and 1.5.

The vorticity generation is described by the vorticity transport equation, Eq. (2). The vorticity production is mainly contributed by the dilation term associated with the dilation $\nabla \cdot \boldsymbol{V}$ multiplied by the vorticity and the baroclinic term due to the misalignment of the pressure and density gradients. We will not discuss the first term of $(\boldsymbol{\omega} \cdot \nabla)\boldsymbol{V}$ and other terms, and will concentrate on the vorticity production contributed by the dilation term and the baroclinic term. Figure 5 shows the vorticity distributions contributed by the dilation effect and the baroclinic term at different instants for the $M_S = 1.5$ case. Figures 5a–5c show the values of the dilation $\nabla \cdot \boldsymbol{V}$, and Figs. 5d–5f for the baroclinic term, as the second shock passed through the induced vortex rings. Moreover, it was found that the vorticities in an absolute value near vortex centers are greater than unity for cases A–C, as seen from Fig. 4. From Figs. 5a–5f, we see that the absolute peak values of the dilation are larger than those for the baroclinic term. Thus the dilation term contributes more than the baroclinic term. Figures 5a and 5d show the values of the dilation and the baroclinic term before the second shock/vortex interaction, Figs. 5b and 5e during the interaction, and Figs. 5c and 5f after the interaction. During the interaction, the peak values of the dilation and the baroclinic term are largely increased. After the interaction, the values of the dilation always decrease from $t = 3.5$ to 3.9, similarly

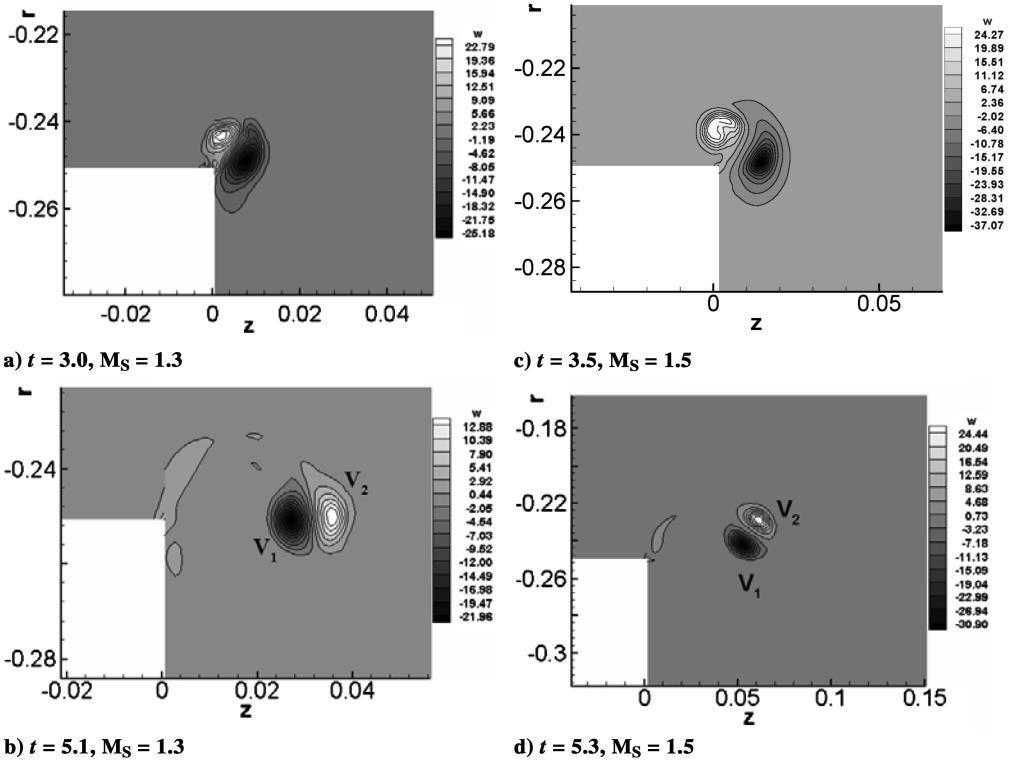

Fig. 4 Vorticity contours at different instants (case A).

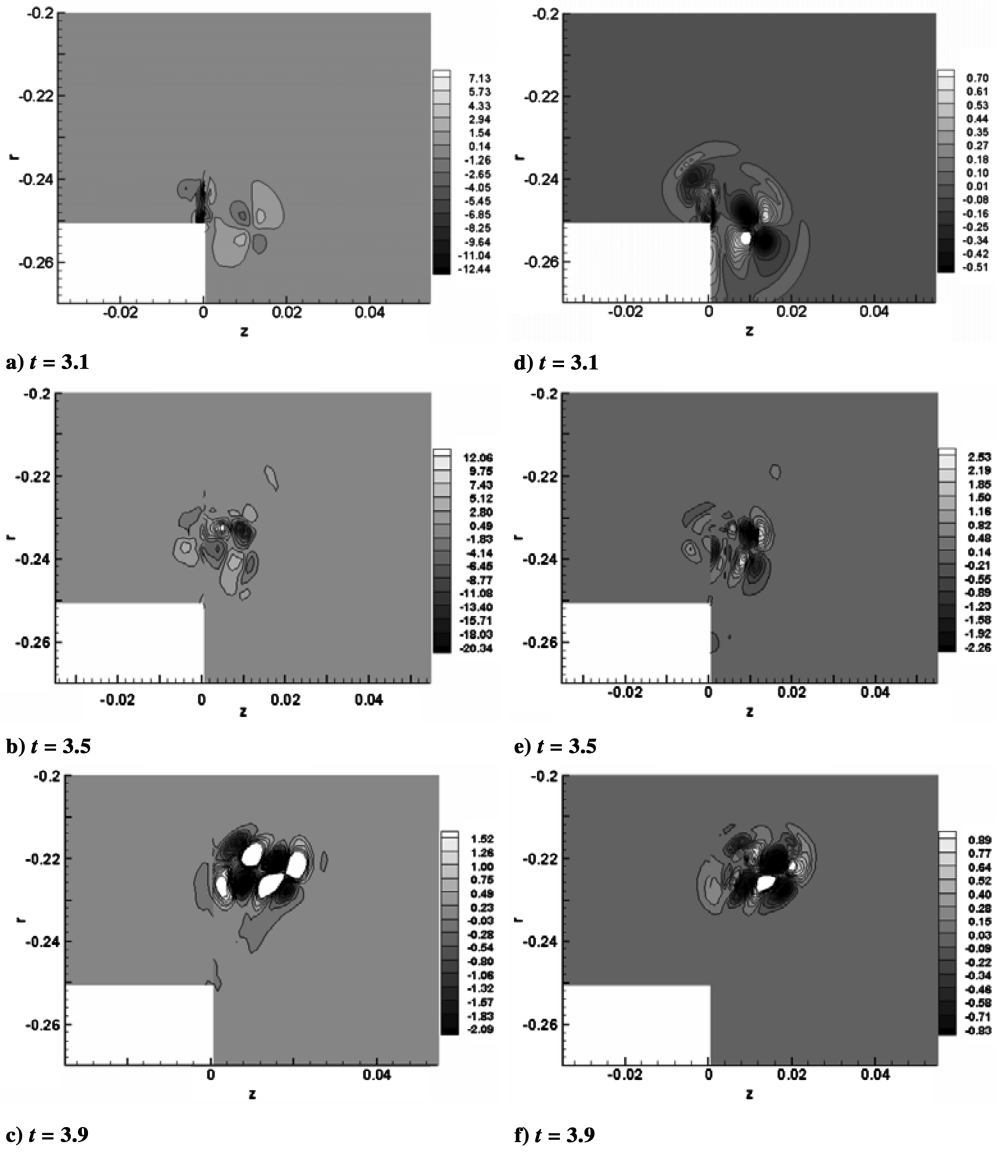

Fig. 5 Value distributions of a)–c) the dilation ($\nabla \cdot V$) and d)–f) the baroclinic term at different instants, $M_S = 1.5$ (case A).

for the baroclinic term, as shown in Figs. 5b, 5c, 5e, and 5f. This means that the pair of vortex rings has been weakened by the second shock wave after its passage. In summary, the dilation term plays a more important role in the vorticity production than the baroclinic term. In the same vein, similar results to Fig. 5 occur for the reflected shock/ring-vortices interaction for later times.

The variation of the flow circulation enclosed by the region $\{(r, \theta, z)| -0.25 < r < -0.076, \quad -0.174 < z < 0$, and $-0.076 < r < 0, \ 0 < z < 0.174\}$ is shown in Fig. 6. The circulation of the vortical flow caused by the primary shock wave increases to a maximum value at about $t = 2.2$ before the second shock approaches to the induced ring vortices. As the second shock approaches to the vortex rings, staring to interact with, the circulation monotonically decreases. At about $t = 3.6$, after interaction, the circulation is almost a constant value, until the arrival of the reflected shock wave at about $t = 5.0$. For $t > 5.0$, the circulation is slightly decreased because of the effect of the reflected shock wave.

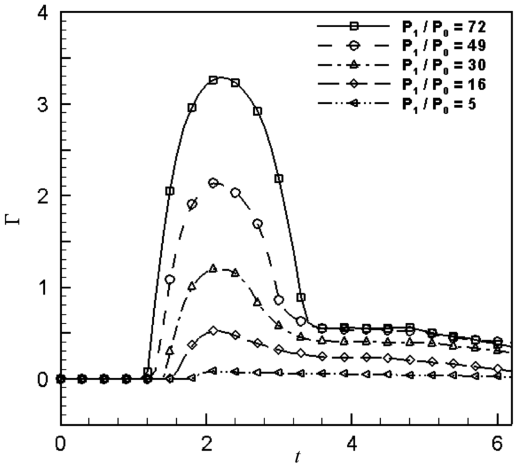

Fig. 6 The circulation variation versus time for different blast-wave intensities, $M_S = 1.5$ (case A).

C. Viscous Effects

To study the viscous effects, the laminar and turbulent-flow models are used. More grid points are clustered near the wall and the sudden expansion. The minimum grid size of 5×10^{-4} is chosen for the laminar-flow case, and 3×10^{-4} for the turbulent-flow case. The turbulence model used is a two-layer algebraic eddy viscosity turbulence model. The Reynolds number is chosen to be 250,000. It was found that the flow structures obtained from the viscous-flow models are almost the same as that obtained from the inviscid-flow model. However, there is a small difference in the ring-vortex intensity. Figure 7 shows the minimum pressures at the major vortex

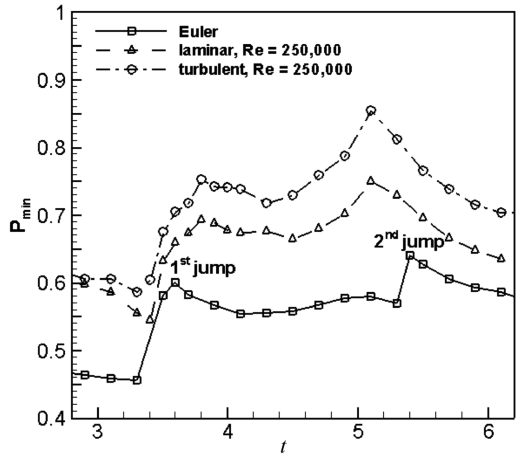

Fig. 7 Comparison of the minimum pressures at the major ring vortex centers from $t = 2.9$ to 6.1 for different flow models, $p_1/p_0 = 72$ (case A).

centers at different instants for different flow models for case A. One can see that the first and second jumps in the minimum pressures are steeper than those for the viscous-flow models. Moreover, the minimum pressures for the inviscid-flow model can be 8–23% and 14–32% lower than those for the corresponding laminar and turbulent-flow models at some instants, respectively. Obviously the induced vortex rings for the viscous-flow models are weaker than those for the inviscid-flow model, because of energy dissipation due to the viscosity. For the viscous-flow models, the induced ring vortices in the turbulent-flow model are at most 17% weaker than that for the laminar-flow model, causing at most a 12% pressure difference at vortex centers. Moreover, the second shock/ring-vortex interaction took place earlier than those in the viscous-flow models because of the faster shock speed in the inviscid-flow model. However, the reflected shock/ring-vortex interaction in the inviscid-flow model took place later than that in the viscous-flow model. This is because a regular reflection occurred in the inviscid-flow model, but a Mach reflection happened in the viscous-flow models, as shown in Fig. 8. From Fig. 8, one can see that the reflected shock in the laminar flow is closer to the vortex rings than that in the inviscid-flow model. The trajectories of the vortex centers can be affected by the viscosity. Figure 9 shows the comparison of the trajectories of the major ring-vortex centers for different flow models. We can see that before $t = 5.2$, three trajectories predicted by three flow models are almost the same. At about $t = 5.3$ the two trajectories in the viscous-flow models move upstream and toward the duct centerline, but the trajectory in the inviscid-flow model continuously moves downstream. The reason for the trajectory turn is that a third vortex ring near the sudden expansion is developed in the viscous-flow models, which is not clearly seen in the inviscid-flow model.

D. Case B: Simultaneous Interaction of the Second and Reflected Shocks with the Induced Vortex Rings

To have a simultaneous interaction of the second and reflected shock waves with the induced vortex rings, the duct's expansion ratio is chosen to be 1.57 for $M_S = 1.5$ ($p_1/p_0 = 72$). The arrival times of the 1st, 2nd, and reflected shock waves at the sudden expansion are 1.2, 3.4, and 3.2, respectively, for inviscid- and viscous-flow models. Figure 10 shows the variation of the minimum pressures at the major ring-vortex centers for different flow models. We see that there is a sharp jump after the passage of the second and reflected shock waves between $t = 3.1$ to 3.5. But the second jump is not as sharp as the first jump. The difference of vortex-center pressures between the inviscid- and laminar flows ranges from 12–29%, and 20–32% for the pressure difference between the inviscid and turbulent flows. Clearly, the inviscid-flow model overpredicted the vortex-center pressures. The trajectories of the major ring-vortex centers for cases A–C are different. In case B, the reflected shock wave is stronger than that in case A, resulting in a trajectory's upstream movement for inviscid flows and a centered movement for viscous

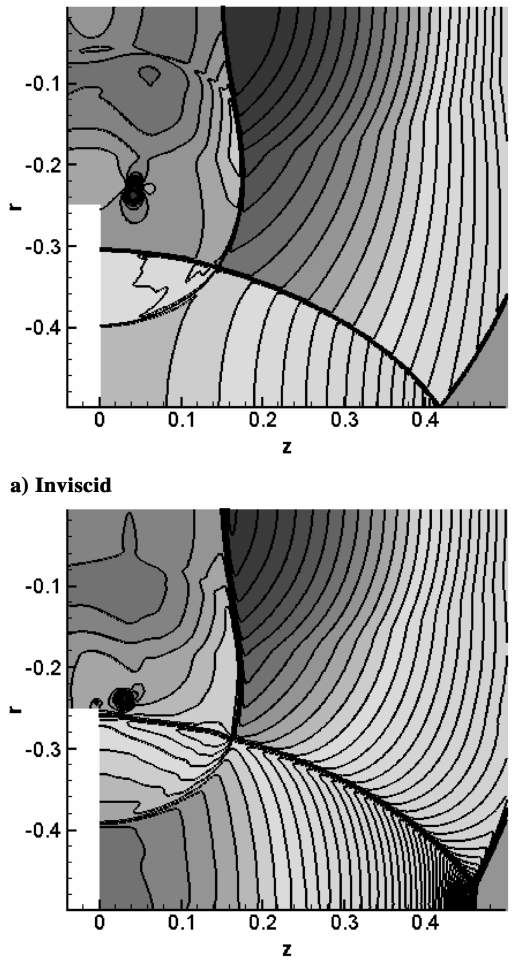

Fig. 8 Comparison the flow pattern of pressure distribution for different flow models, $t = 4.8$, $p_1/p_0 = 72$ (case A).

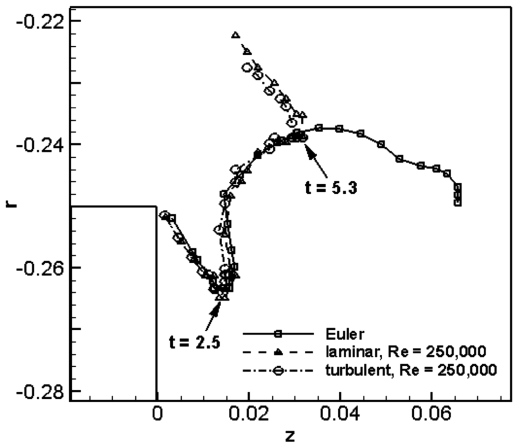

Fig. 9 Comparison of the trajectories at the major ring vortex centers from $t = 1.3$ to 6.5 with $\Delta t = 0.2$ for different flow models, $p_1/p_0 = 72$ (case A).

flows at some critical times. It was found that a third ring vortex near the sudden expansion may be induced, which is visible for the inviscid-flow case through the display of the computational schlieren picture as shown in Fig. 11.

E. Case C: Reflected Shock/Ring-Vortex Interaction After the Second Shock/Ring-Vortex Interaction

This case represents the reflected shock wave arrives at the sudden expansion earlier than the second shock wave. To achieve this, the

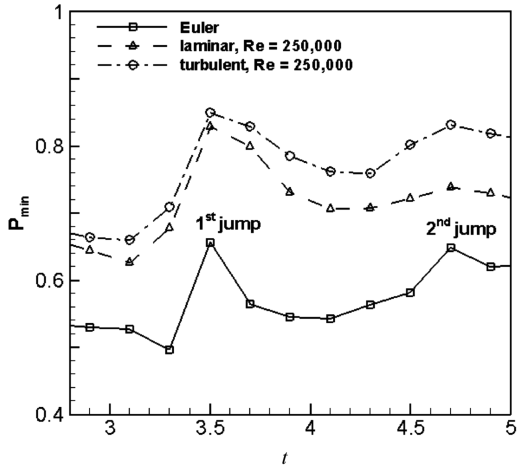

Fig. 10 Comparison of the pressures at major ring vortex centers from $t = 2.9$ to 4.9 for different models, $p_1/p_0 = 72$ (case B).

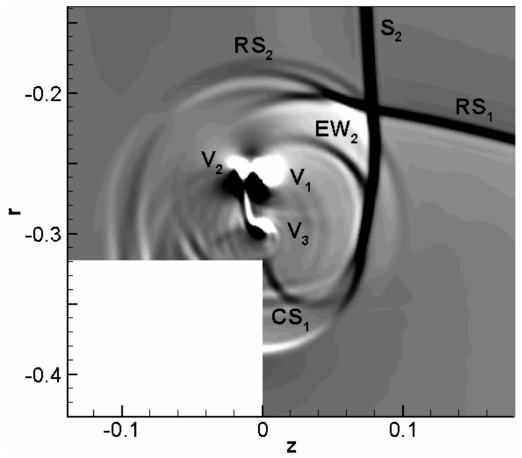

Fig. 11 The computational schlieren picture of the third ring vortex for the inviscid-flow case, $p_1/p_0 = 72$, $t = 3.9$ (case B).

duct expansion ratio is reduced to 1.23. The chosen values of flow parameters are tabulated in Table 1. A prominent flow feature is that a second pair of ring vortices V_3 and V_4 may be induced by the reflected shock wave, as V_1 and V_2 induced by the primary shock wave, as shown in Fig. 12 for the case of a turbulent flow with $p_1/p_0 = 72$. As mentioned in Sec. III.B, the passage of the reflected and second shock waves can weaken the vortex rings, resulting in minimum pressure increases at the vortex centers. Figure 13 shows the effect of the second shock wave on the minimum pressure variation at the major ring-vortex centers for different blast-wave intensities. From Fig. 13, we can see two big jumps. In particular, the second jump is sharp for stronger blast waves for three flow models. Because of the viscous dissipation, the turbulent-flow model predicts an about 38% higher vortex-center pressure at $t = 3.9$ than that for the inviscid-flow model, and about 37% for the laminar-flow model at $t = 4.3$. The earlier arrival of the reflected shock wave than the second shock wave has an effect on the trajectories of the vortex centers. Figure 14 shows the trajectories of the major ring-vortex centers at different instants, predicted by different models for $p_1/p_0 = 72$ and $Re = 250,000$ for viscous flows. As seen from Fig. 14, the trajectory history is quite complicated. However, a common feature is that at the first critical time, $t = 1.9$ for the inviscid-flow case and $t = 2.1$ for the viscous-flow case, while expansion waves move upstream, the vortex centers start to move upstream and toward the duct centerline. After the critical time $t = 2.5$, the trajectories of the major ring vortex centers for the viscous-flow case are closer to the core stream than that for the inviscid-flow case. The reason is that a minor vortex ring (V_3) is developed near the convex corner. The strength of the minor vortex ring (V_3) for the inviscid-flow case is stronger than that for the

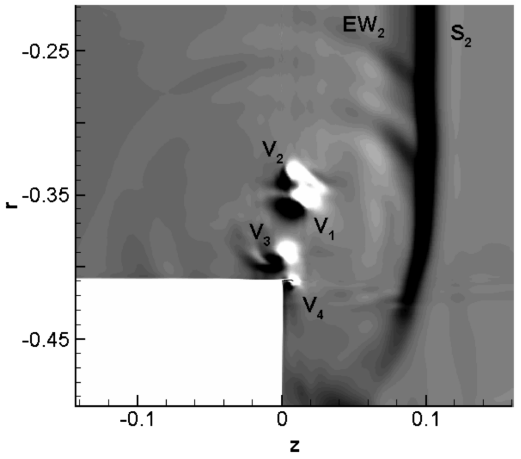

Fig. 12 The computational schlieren picture of two-pair ring vortices of a turbulent flow in case C, $p_1/p_0 = 72$, $t = 3.9$, $Re = 250,000$.

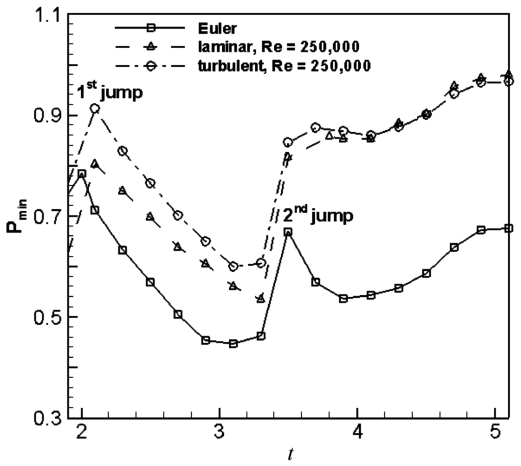

Fig. 13 Comparison of the pressures at major ring vortex centers from $t = 1.9$ to 5.1 for different flow models, $p_1/p_0 = 72$ (case C).

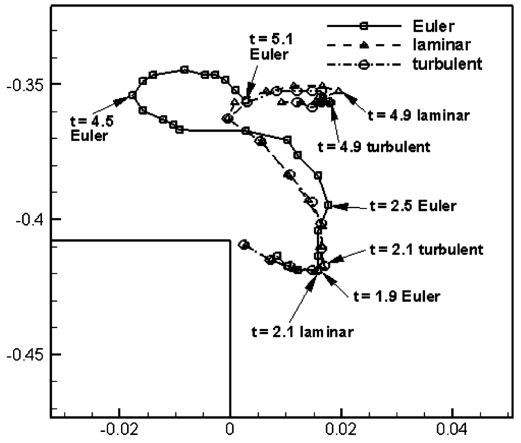

Fig. 14 Comparison of the trajectories at major vortex centers form $t = 1.4$ to 5.5 with $\Delta t = 0.2$ for different flow models, $p_1/p_0 = 72$, $Re = 250,000$ for viscous flows (case C).

viscous-flow case. And so, the trajectories of the major ring-vortex centers for the viscous flow are closer to the core stream than those for the inviscid flow. After the second critical time, these vortex rings move downstream.

IV. Conclusions

A high-resolution numerical method is used to solve the axisymmetric, unsteady compressible Euler/Navier–Stokes equations. The present solver is validated to be reasonably accurate for several test flow problems. The problem of different intensity blast waves propagating in a circular duct with a sudden expansion with different expansion ratios is numerically investigated in detail, depending on the time sequence of the second shock and the reflected shock arriving at the pair of vortex rings induced by the primary shock wave. To study blast-wave/ring-vortex interactions, we use two techniques of computational shadowgraph and computational schlieren picture. It was found that the method of computational schlieren picture is better for identifying flow structures induced by shock/ring-vortex interactions.

The mechanism of vorticity generation in the suddenly expanded circular duct is studied in detail. The second and reflected shock waves play an important role in the vorticity generation process for blast/ring-vortex interactions. It is found that, in the vorticity transport equation during the second and reflected shocks/ring-vortex interactions, the contribution of the term due to the dilation effect is more than the baroclinic term.

It is found that the mutual influence of the second and reflected shocks interacting with the induced vortex rings by the primary shock wave, results in a pressure increase at the vortex centers after shock-wave passing and in weakening the induced vortex rings. Moreover, the trajectories of the major and minor vortex centers may be affected by the expansion waves and a third pair of vortex rings (V_3 and V_4) or a single ring vortex (V_3). In case A, the second pair of the vortex ring can result in an upstream turn of the trajectory at some critical time for viscous-flow models, but not in the invicid-flow model.

The present result shows that the intensities of the major vortex ring are overpredicted by the inviscid-flow model, resulting in 14–32% lower pressures at the major ring vortex centers at some instants in the inviscid flow compared with the turbulent flow for case A, 20–32% for case B, and 21–38% for case C. We also found that the vortex strength generated in the laminar flow is stronger than that for the corresponding turbulent flow, consequently occasionally producing a roughly 12% lower vortex-center pressure for the laminar flow than that for the corresponding turbulent flow for cases A–C.

Acknowledgment

The support of NSC 93-2213-E006-126 for this study is gratefully acknowledged.

References

[1] Skews, B. W., "The Perturbed Region Behind a Diffracting Shock Wave," *Journal of Fluid Mechanics*, Vol. 29, No. 4, 1967, pp. 705–719.

[2] Hillier, R., "Computation of Shock Wave Diffraction at a Ninety-Degree Convex Edge," *Shock Waves*, Vol. 1, No. 2, 1991, pp. 89–98.

[3] Liang, S. M., and Lo, C. P., "Shock/Vortex Interactions Induced by Blast Waves," *AIAA Journal*, Vol. 41, No. 7, 2003, pp. 1341–1346.

[4] Ben-Dor, G., *Shock Wave Reflection Phenomena*, Springer–Verlag, New York, 1992.

[5] Takayama, K., and Jiang, Z., "Shock Wave Reflection over Wedges: A Benchmark Test for CFD and Experiments," *Shock Waves*, Vol. 7, No. 4, 1997, pp. 191–203.

[6] Sun, M., and Takayama, K., "A Note Numerical Simulation of Vortical Structures in Shock Diffraction," *Shock Waves*, Vol. 13, No. 1, 2003, pp. 25–32.

[7] Sun, M., and Takayama, K., "Vorticity Production in Shock Diffraction," *Journal of Fluid Mechanics*, Vol. 478, March 2003, pp. 237–256.

[8] Kim, H. D., and Setoguchi, T., "Study of the Discharge of Weak Shocks from an Open End of a Duct," *Journal of Sound and Vibration*, Vol. 226, No. 5, 1999, pp. 1011–1028.

[9] Jiang, Z., Onodera, K., and Takayama, K., "Evolution of Shock Waves and the Primary Vortex Loop Discharged from a Square Cross-Sectional Tube," *Shock Waves*, Vol. 9, No. 1, 1999, pp. 1–10.

[10] Abate, G., and Shyy, W., "Dynamic Structure of Confined Shocks Undergoing Sudden Expansion," *Progress in Aerospace Sciences*, Vol. 38, No. 1, 2002, pp. 23–42.

[11] Howard, L., and Mathews, D., "On the Vortices Produced in Shock Diffraction," *Journal of Applied Physics*, Vol. 27, No. 3, 1956, pp. 223–231.

[12] Bazhennova, T. V., Gvozdeva, L. G., and Nettleton, M. A., "Unsteady Interactions of Shock Waves," *Progress in Aerospace Sciences*, Vol. 21, No. 1, 1984, pp. 249–331.

[13] Mandella, M., Moon, Y. L. and Bershader, D., "Quantitative Study of Shock generated Compressible Vortex Flows," *Proceedings of the 15th International Symposium on Shock Waves and Shock Tubes*, Stanford Univ. Press, Stanford, CA, 1986, pp. 471–477.

[14] Yang, J., Onodera, O., and Takayama, K., "Holographic Interferometric Investigation of Shock Wave Diffraction," *Journal of the Visualization Society of Japan*, Vol. 14, No. 1, July 1994, pp. 85–88.

[15] Uchiyama N., and Inoue, O., "Shock Wave/Vortex Interaction in a Flow over 90-deg Sharp Corner," *AIAA Journal*, Vol. 33, No. 9, 1995, pp. 1740–1743.

[16] Gröing, H., "Shock Wave/Vortex Interaction," *Proceedings of the Second International Workshop on Shock Wave/Vortex Interaction*, Tohoku Univ., Sendai, Japan, 1998, pp. 1–14.

[17] Dosanjh, D. S., and Weeks, T. M., "Interaction of a Starting Vortex as Well as a Vortex Street with a Traveling Shock Wave," *AIAA Journal*, Vol. 3, No. 2, Feb. 1965, pp. 216–223.

[18] Ellzey J. L., and Henneke, M. R., "The Shock-Vortex Interaction: The Origins of the Acoustic Wave," *Fluid Dynamics Research*, Vol. 21, No. 3, 1997, pp. 171–184.

[19] Grasso, F., and Pirozzoli, S., "Shock-Wave-Vortex Interactions: Shock and Vortex Deformations, and Sound Production," *Theoretical and Computational Fluid Dynamics*, Vol. 13, No. 6, 2000, pp. 421–456.

[20] Meadows, K. R., Kumar, A., and Hussaini, M. Y., "Computational Study on the Interaction Between a Vortex and a Shock Wave," *AIAA Journal*, Vol. 29, No. 2, 1991, pp. 174–179.

[21] Ellzey, J. L., Henneke, M. R., Picone, J. M., and Oran, E. S., "The Interaction of a Shock with a Vortex: Shock Distortion and the Production of Acoustic Waves," *Physics of Fluids*, Vol. 7, No. 1, 1995, pp. 172–184.

[22] Guichard, L., Vervisch, L., and Domingo, P., "Two-Dimensional Weak Shock-Vortex Interaction in a Mixing Zone," *AIAA Journal*, Vol. 33, No. 10, 1995, pp. 1797–1802.

[23] Chatterjee, A., "Shock Wave Deformation in Shock-Vortex Interactions," *Shock Waves*, Vol. 9, No. 2, 1999, pp. 95–105.

[24] Inoue, O., and Takahashi, Y., "Successive Generation of Sounds by Shock-Strong Vortex Interaction," *Physics of Fluids*, Vol. 12, No. 12, 2000, pp. 3229–3244.

[25] Chang, K. S., and Kim, J. K., "Numerical Investigation of Inviscid Wave Dynamics in an Expansion Tube," *Shock Waves*, Vol. 5, No. 1/2, 1995, pp. 33–45.

[26] Jiang, Z., Takayama, K., Babinsky, H., and Meguro, T., "Transient Shock Wave Flows in Tubes with a Sudden Change in Cross Section," *Shock Waves*, Vol. 7, No. 3, 1997, pp. 151–162.

[27] Chen, H., and Liang, S. M., "Planar Blast/Vortex Interaction and Sound Generation," *AIAA Journal*, Vol. 40, No. 11, 2002, pp. 2298–2304.

[28] Kleine, H., Ritzerfeld, E. and Grönig, H., "Shock Wave Diffraction at a Ninety Degree Corner," *Computational Fluid Dynamics Journal*, Vol. 12, No. 2, 2003, pp. 142–158.

[29] Hoffmann, K. A., and Chiang, S. T., *Computational Fluid Dynamics for Engineers*, Vol. 2, Engineering Education System™, Wichita, KS, 1993.

[30] Baldwin, B., and Lomax, H., "Thin-Layer Approximation and Algebraic Model for Separated Turbulent Flows," AIAA Paper 78-257, 1978.

[31] Jiang, G.-S., and Shu, C.-W., "Efficient Implementation of Weighted ENO Schemes," *Journal of Computational Physics*, Vol. 126, No. 1, 1996, pp. 202–228.

[32] Shu, C. W., and Osher, S., "Efficiently Implementation of the Essentially Non-Oscillatory Shock-Capturing Schemes 2," *Journal of Computational Physics*, Vol. 83, No. 1, 1989, pp. 32–78.

[33] Thompson, K. W., "Time Dependent Boundary Conditions for Hyperbolic Systems 2," *Journal of Computational Physics*, Vol. 89, No. 2, 1990, pp. 439–461.

[34] Liao, C. Y., "Numerical Investigation of Blast Wave/Vortex Interaction in a Duct with a Sudden Expansion," Ph.D. Dissertation, Department of Aeronautics and Astronautics Engineering, National Cheng Kung University, Tainan, Taiwan, Jan. 2005.

[35] Hakkinen, R. J., Greber, L., and Abarbanel, S. S., "The Interaction of an Oblique Shock Wave with a Laminar Boundary Layer," NASA Memo 2-18-59W, 1959.

[36] Yang, J., "Experimental and Theoretical Study of Weak Shock Wave," Ph.D. Dissertation, Institute of Fluid Science, Tohoku University, Sendai, Japan, 1995.
[37] White, F. M., *Viscous Fluid Flow*, 2nd ed., McGraw–Hill, New York, 1991, p. 300.
[38] Anon., *Tecplot User's Manual*, 9th ed., Amtec Engineering, Inc., Bellevue, WA, 2001.
[39] Deschambault, R. L., and Glass, I. I., "An Update on Non-Stationary Oblique Shock-Wave Reflections: Actual Isopycnics and Numerical Experiments," *Journal of Fluid Mechanics*, Vol. 31, June 1983, pp. 27–57.

C. Kaplan
Associate Editor